Terahertz Spectroscopy of Plasmonic Fractals

A. Agrawal,[1] T. Matsui,[2,*] W. Zhu,[1] A. Nahata,[1] and Z. V. Vardeny[2]

[1]*Department of Electrical and Computer Engineering, University of Utah, Salt Lake City, Utah 84112, USA*
[2]*Physics Department, University of Utah, Salt Lake City, Utah 84112 USA*

We use terahertz time-domain spectroscopy to study the transmission properties of metallic films perforated with aperture arrays having deterministic or stochastic fractal morphologies (''plasmonic fractals''), and compare them with random aperture arrays. All of the measured plasmonic fractals show transmission resonances and antiresonances at frequencies that correspond to prominent features in their structure factors in **k** space. However, in sharp contrast to periodic aperture arrays, the resonant transmission enhancement decreases with increasing array size. This property is explained using a density-density correlation function, and is utilized for determining the underlying fractal dimensionality, $D(<2)$. Furthermore, a sum rule for the transmission resonances and antiresonances in plasmonic fractals relative to the transmission of the corresponding random aperture arrays is obtained, and is shown to be universal.

Light localization using periodic or disordered media has been a topic of scientific interest for several decades, and is considered to be a consequence of strong interference of light in the underlying media [1–9]. For example, by engineering the structural defects in photonic crystals, intense light localization with very high Q can be observed [4]. Also, by using randomly distributed strong light scatterers, Anderson localization of light can be induced with confinement on a subwavelength scale [5–8]. The recent emergence of fractal structures has also attracted significant interest in the optical community because of the possibility of obtaining light confinement. Fractal structures are unique in that they have a very high degree of self-similarly (also referred to as ''dilation symmetry''); i.e., they are exactly or approximately similar to a part of themselves [10]. Light scattering from objects with fractal morphology such as colloidal aggregates, self-affine surfaces, and semicontinuous thin films has been extensively studied to demonstrate the ability of obtaining intense light localization [11–19]. However, a deeper understanding is critical for developing novel devices and technologies based on these optical self-similar structures.

We report terahertz (THz) transmission resonances from several aperture arrays in metallic films exhibiting fractal geometries, for both deterministic and stochastic fractal morphologies. We refer to these self-similar metal based structures exhibiting unique fractal characteristics as ''plasmonic fractals.'' We found that transmission resonances and antiresonances also form in these complex structures, at frequencies that closely match prominent features in their structure factor in **k** space [20]. However in contrast to periodic plasmonic lattices, where the transmission resonances are accentuated and increase with lattice size, the resonant transmission enhancement in plasmonic fractals decreases with the structure size. This is explained by a density-density correlation function, and is

used to further characterize the plasmonic fractals morphology.

Fractal morphologies are characterized by a parameter referred to as the fractal dimension, D, which is smaller than the topological dimension, D^* [10]. D is a statistical quantity that gives an indication of how completely a fractal structure appears to fill the available space. D is typically calculated from the structure topography using the following expression [21]:

$$N = k_0\left(\frac{R_g}{a}\right)^D, \qquad (1)$$

where N is the number of primary particles in the aggregate, which is proportional to the mass (or filled ''volume''), R_g is a measure of the aggregate radius (or gyration radius), a is the monomer radius, and k_0 is a proportionality constant of order unity.

Fractal structures can be generated using both deterministic and stochastic approaches. The deterministic approach exhibits exact self-similarity; examples of such structures include Sierpinski carpet, Vicsek fractal, hexaflake (HF), etc. [22,23]. In contrast, the stochastic approach is used to generate fractal structures that exhibit statistical self-similarity; examples include structures that are formed by diffusion-limited aggregation (DLA), ballistic aggregation (BA), etc. [24–26]. The real and reciprocal space representations of three fractal structures, namely, the HF, BA, and DLA fractals used in our study, are shown in Fig. 1. The stochastic fractal structures (BA and DLA) were designed using an aggregation process in which the nearest neighbor distance, d, and the aperture size were preserved [27]. We used two sets of samples: one set consisted of the plasmonic fractals, while the other set consisted of randomly distributed holes (RHs) having the same number of apertures as the corresponding fractal structures. The three plasmonic fractals were fabricated
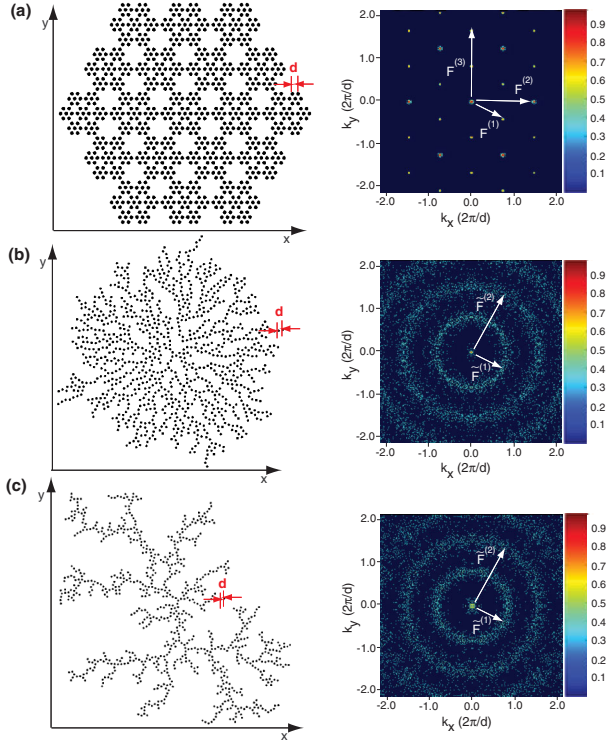
FIG. 1 (color online). The real (left panels) and reciprocal space (right panels) representations of deterministic (a) and stochastic (b) and (c) plasmonic fractals used in our study, where the black dots correspond to the location of apertures having fixed average spacing $d = 1.0$ mm and aperture radius $a = 300$ μm. (a) HF fractal, (b) BA, and (c) DLA fractal. The discrete reciprocal vectors (RVs) in $\mathbf{k}$ space, $F^{(i)}$ in (a), and diffused $\tilde{F}^{(i)}$ in (b) and (c) are assigned.
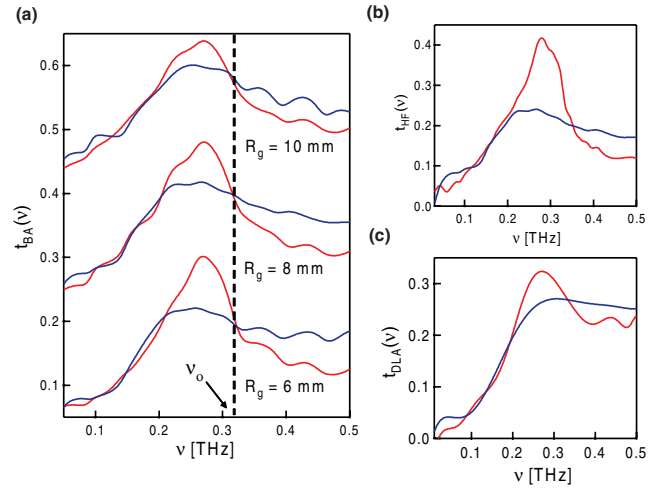

FIG. 2 (color online). Normalized THz transmittance spectra, $t(\nu)$, for the plasmonic fractals shown in Fig. 1 [lighter (red) solid line], compared to $t_0(\nu)$ of the corresponding RH [darker (blue) solid line] aperture arrays. (a) $t(\nu)$ and $t_0(\nu)$ of BA fractal and respective RH array at three different gyration radii (R_g). The isosbestic frequency $\nu_0 = 0.33$ THz is assigned by a vertical broken line. (b) and (c) $t(\nu)$ and $t_0(\nu)$ of HF and DLA plasmonic fractals for $R_g = 22$ mm and 35 mm, respectively.

on 75 μm thick freestanding stainless steel films, where the dots were replaced with circular apertures having spacing $d = 1.0$ mm and radius $a = 300$ μm. The structure factor in $\mathbf{k}$ space was calculated using two-dimensional Fourier transforms of the real space structures, and reveals various reciprocal vectors (RVs). Figure 1(a) shows discrete RVs (labeled $F^{(i)}$), associated with the HF deterministic fractal, which are similar to reciprocal lattice vectors found in periodic structures. However the $\mathbf{k}$-space representation of the BA and DLA stochastic fractals [Figs. 1(b) and 1(c), respectively] are characterized by continuous concentric diffused streaks (labeled $\tilde{F}^{(i)}$), which are similar to features observed in the $\mathbf{k}$-space representation of liquid and amorphous materials [28].

We used standard THz time-domain spectroscopy to measure the normalized THz electric field transmission, $t(\nu)$, through these structures [27]. For measuring $t(\nu)$ vs R_g, a circular aperture having a controlled radius was placed in front of the sample. Figure 2(a) shows $t(\nu)$ through a BA fractal compared to the spectrum, $t_0(\nu)$ of a corresponding RH sample, for three R_g's. $t(\nu)$ contain three remarkable features: (i) even though the BA fractal has no discrete RVs in $\mathbf{k}$ space, $t(\nu)$ still shows resonantly

enhanced bands relative to $t_0(\nu)$; (ii) $t(\nu)$ also exhibits antiresonant reduction bands at higher corresponding frequencies; (iii) surprisingly, with increasing R_g the resonant transmission, t_{max}, decreases with respect to $t_0(\nu)$. Point (iii) is counterintuitive because the number of apertures that participate in forming the resonant transmission increases with R_g and this leads to a more accentuated transmission band in periodic hole arrays [29,30]. We note that $t_0(\nu)$ of the RH samples (Fig. 2) has slightly different R_g than the corresponding fractal structures for maintaining constant N. Figures 2(b) and 2(c) show $t(\nu)$ of the two other plasmonic fractals, namely, HF and DLA, along with $t_0(\nu)$ of the corresponding RH samples. $t(\nu)$ here exhibit trends similar to those observed in $t(\nu)$ of the BA sample, namely, a resonantly enhanced transmission and a corresponding antiresonance reduction with respect to $t_0(\nu)$. This shows that resonant transmission in plasmonic fractals is universal, regardless of the type of fractal morphology (deterministic or chaotic); this is similar to resonant transmission through other aperture arrays having periodic or quasiperiodic morphology [9,31].

We devised a method to obtain the fractal dimensionality, D, from the dependence of $t(\nu)$ on R_g, as shown in Fig. 3(a). Using RH samples, we previously demonstrated that $t(\nu)$ scales linearly with the number of sampled apertures, N [31]. Thus, we can simplify Eq. (1) to obtain D from the slope of the following functional dependence:

$$D \propto \left(\frac{\log(N)}{\log(R_g/a)} \right) \propto \left(\frac{\log(t_{\nu_o})}{\log(R_g/a)} \right). \qquad (2)$$

Here t_{ν_o} is the transmission value at the isosbestic frequency, ν_o, at which $t(\nu)$ of the fractal array and corre-
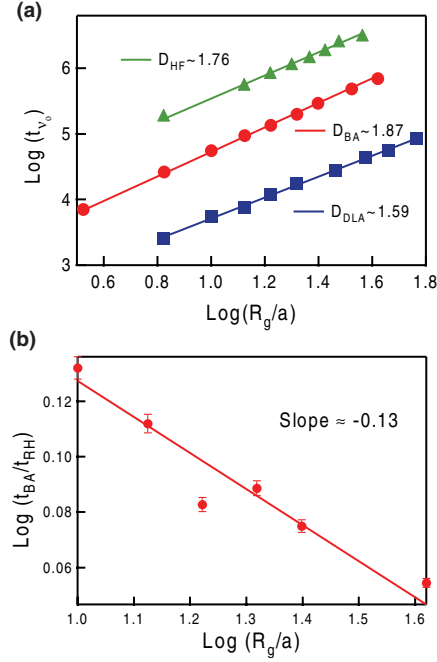
(a)

(b)

FIG. 3 (color online).   (a) Fractal dimensionality (D) of the three fractal structures shown in Fig. 1 as extracted from the THz transmittance value, t_{ν_o} at the isosbestic frequency ($\nu_0 = 0.33$ THz), which is plotted vs the gyration radius (R_g). The obtained D values are given. (b) The ratio of resonantly enhanced transmittance maximum, t_{max} of the BA plasmonic fractal and $t_0(\nu_{max})$ of the corresponding RH array, plotted vs R_g. The resulting slope of -0.13 is consistent with the model calculation and D_{BA} extracted in (a).

sponding RH array cross each other [see Fig. 2(a)]; therefore, t_{ν_o} is solely determined by N, and does not incorporate the resonance effect induced by the underlying structure factor. We note that ν_o mainly depends on the aperture cutoff properties (its radius, a), and is therefore independent of R_g [31]. In Fig. 3(a) we plot $\log(t_{\nu_o})$ vs $\log(R_g/a)$ for the three plasmonic fractals shown in Fig. 1. From the resulting slopes we obtain the following D values using Eq. (2): $D_{HF} = 1.76$, $D_{BA} = 1.87$, and $D_{DLA} = 1.59$. These values are in excellent agreement with D values predicted by the theory, namely, $D_{HF} = 1.77$, $D_{BA} = 1.88$, and $D_{DLA} = 1.61$ [22–27].

The unusual resonant enhancement property in plasmonic fractals, where t_{max} decreases with increasing R_g [Fig. 2(a)], may be explained using the density-density correlation function, $p(\mathbf{r}; \mathbf{r}')$, and its Fourier transform, which is the essence of the structure factor that determines the transmission properties [21]. Qualitatively, $p(\mathbf{r}; \mathbf{r}')$ corresponds to the probability, p, of finding another monomer at point $\mathbf{r}'$ if there is a monomer at point $\mathbf{r}$. This function can be reformulated to depend only on the radius vector $\mathbf{r}'-\mathbf{r}$, namely, $p(\mathbf{r}'-\mathbf{r})$. Since the aperture nearest neighbor distance, d, for the fractal structures is fixed by the fabrication process, we expect a maximum in $p(\mathbf{r}'-\mathbf{r})$ at $|\mathbf{r}'-\mathbf{r}| = d$. This generates a maximum in the structure factor in the

form of a ring in $\mathbf{k}$ space at a radius $k = 2\pi/d$ [see Figs. 1(b) and 1(c) for the stochastic fractals), which determines the transmission peak, t_{max}, that occurs at $\nu_{max} = c2\pi/d$. Therefore, t_{max} is proportional to the probability p at $|\mathbf{r}'-\mathbf{r}| = d$, which, in turn, is determined by the number of aperture pairs, N_p, within the fabricated structure. Since d is fixed, then N_p is proportional to N within the structure. For fractals, this probability depends on the structure size (or R_g), because N does not grow with R_g according to the geometrical dimension, D^*, but rather, N grows with R_g according to the fractal dimensionality, D [Eq. (1)]. Since the aperture radius is also fixed in the fabricated arrays, the probability of finding an aperture within the radius R_g in the fractals may be obtained by the ratio, P, of the area covered by the apertures (A_{Frac}) to the entire area (A_{Total}):

$$P = \frac{A_{Frac}}{A_{Total}} = \frac{N\pi a^2}{\pi R_g^2}. \tag{3}$$

Since $N \propto (R_g/a)^D$ [Eq. (1)], we can simplify Eq. (3) to read

$$P \propto \left(\frac{R_g}{a}\right)^{D-2}. \tag{4}$$

Equation (4) shows that P (and consequently t_{max}) decreases with R_g because $D < 2$ for two-dimensional fractals; this is evident in the data [Fig. 2(a)]. In Fig. 3(b) we plot the experimental enhancement factor, t_{max}/t_0, vs R_g for the BA fractal on a logarithmical scale, and fit the data with a straight line having the slope of $D - 2$ [Eq. (4)], where the value D is directly obtained from Fig. 3(a). The good agreement between the data and fit validates our approach, and explains the curious decrease of t_{max} with R_g, which is unique for fractal structures.

Another observation from the spectra shown in Fig. 2 is that $t(\nu)$ for the plasmonic fractals are modulated around $t_0(\nu)$ of the corresponding RH arrays. For the stochastic fractals $t(\nu)$ are enhanced at resonant frequencies that correspond to the diffused RVs ($\tilde{F}^{(i)}$) seen in the $\mathbf{k}$-space representation of Figs. 1(b) and 1(c), and are simultaneously suppressed at higher frequencies. This is more clearly illustrated by the shaded (yellow) regions in the non-normalized transmission spectra, $T(\nu)$, for the BA and RH arrays shown in Fig. 4(a). In the Fig. 4(a) inset, we plot the ratio, f, of the area under the $T(\nu)$ spectra for the BA array to that of the RH array, as a function of R_g; f fluctuates ~ 0.96. We found that $f \sim 1.0$ for all three plasmonic fractals. To understand this phenomenon we analyzed the structure factor associated with all three plasmonic fractals and corresponding RH arrays [31] in greater detail by obtaining the relative scattering spectral density, $\Sigma_{rel}\tilde{F}^{(i)}(\nu)$, which is the Fourier transform of the density-density correlation function, $p(\mathbf{r}; \mathbf{r}')$. To calculate this function, we numerically integrated the amplitude of the Fourier components $[\Sigma\tilde{F}^{(i)}(k)]$ over the azimuthal
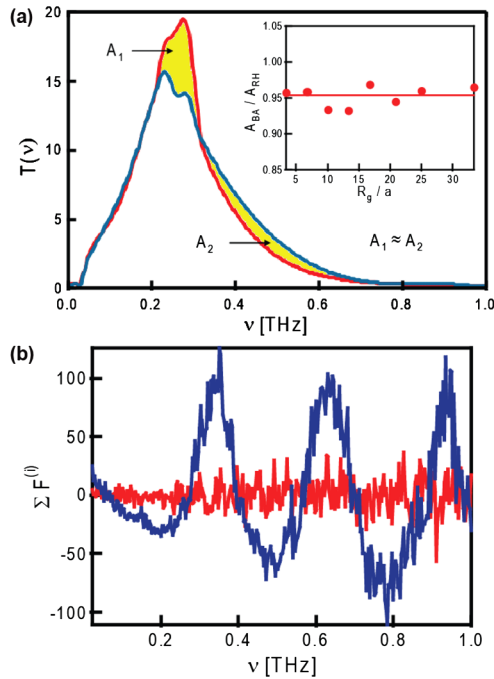
FIG. 4 (color online). Conservation of the integrated THz transmission spectra through the plasmonic fractals. (a) Non-normalized transmission spectra, $T(\nu)$, through BA plasmonic fractal [darker (blue) line] and corresponding RH array structure [lighter (red) line]. The shaded (yellow) regions denote the respective enhanced and suppressed transmission regions in the fractal $T(\nu)$ relative to that of the RH array. Inset: the ratio of area under the curve, A_{BA}/A_{RH}, plotted vs the gyration radius (R_g) for the BA fractal array. (b) The relative scattering spectral density, $\Sigma_{rel}F^{(i)}(\nu)$ (see text for definition), of the BA fractal [darker (blue) line], compared to that of the corresponding RH array [lighter (red) line]. The existence of a sum rule for $\Sigma_{rel}F^{(i)}(\nu)$ integral is evident.

angle (or ring) in **k**-space representation, as a function of $|k|$ (or the corresponding frequency, $\nu = ck$) for the plasmonic fractal, and normalized it by $\Sigma_0\tilde{F}^{(i)}(k)$ of the corresponding RH arrays that was calculated the same way. The spectral density $\Sigma_{rel}\tilde{F}^{(i)}(\nu)$ obtained in this manner is shown for the BA fractal in Fig. 4(b). Surprisingly, we found that the scattering spectral density for the plasmonic fractal is modulated around that of the RH arrays, thus keeping their integrals fixed, similar to their respective transmission spectra. This "sum rule" is consistent with the fabrication process; i.e., if the number of apertures in the fractal and RH structures is kept the same, then the integrated Fourier amplitude of the two structure factors should be exactly equal. Since the resonant transmission properties are determined by the structure factor, the resonant enhancement and related antiresonance suppression in $t(\nu)$ with respect to $t_0(\nu)$ are inherent to the diffraction process, requiring a sum rule that leaves their integrated transmission constant, as seen in the data.

*Permanent address: Department of Electrical and Electronic Engineering, Mie University, Tsu, Mie, 514-8507 Japan.
[1] P. W. Anderson, Phys. Rev. **109**, 1492 (1958).
[2] S. John, Phys. Rev. Lett. **53**, 2169 (1984).
[3] *The Scattering and Localization of Classical Waves*, edited by P. Sheng (World Scientific, Singapore, 1990).
[4] *Photonic Crystals and Light Localization in the 21st Century*, edited by C. M. Soukoulis (Kluwer, Dordrecht, The Netherlands, 2001).
[5] D. S. Wiersma *et al.*, Nature (London) **390**, 671 (1997).
[6] T. Schwartz *et al.*, Nature (London) **446**, 52 (2007).
[7] Y. Lahini *et al.*, Phys. Rev. Lett. **100**, 013906 (2008).
[8] J. Billy *et al.*, Nature (London) **453**, 891 (2008).
[9] D. Pacifici *et al.*, Opt. Express **16**, 9222 (2008).
[10] B. B. Mandelbrot, *The Fractal Geometry of Nature* (W. H. Freeman, San Francisco, 1982).
[11] V. M. Shalaev, M. I. Stockman, and R. Botet, Physica A (Amsterdam) **185**, 181 (1992).
[12] A. K. Sarychev, V. A. Shubin, and V. M. Shalaev, Physica B (Amsterdam) **279**, 87 (2000).
[13] K. Seal *et al.*, Phys. Rev. Lett. **97**, 206103 (2006).
[14] D. P. Tsai *et al.*, Phys. Rev. Lett. **72**, 4149 (1994).
[15] V. M. Shalaev, *Nonlinear Optics of Random Media: Fractal Composites and Metal-Dielectric Films*, Springer Tracts in Modern Physics Vol. 158 (Springer, Berlin, 2000).
[16] V. M. Shalaev *et al.*, Physica A (Amsterdam) **191**, 352 (1992).
[17] D. A. Genov, A. K. Sarychev, and V. M. Shalaev, Phys. Rev. E **67**, 056611 (2003).
[18] S. I. Bozhevolnyi, V. S. Volkov, and K. Leosson, Phys. Rev. Lett. **89**, 186801 (2002).
[19] L. D. Negro, N.-N. Feng, and A. Gopinath, J. Opt. A Pure Appl. Opt. **10**, 064013 (2008).
[20] Y.-J. Bao *et al.*, Appl. Phys. Lett. **90**, 251914 (2007).
[21] C. M. Sorensen, Aerosol Sci. Technol. **35**, 648 (2001).
[22] W. Sierpinski, Comptes Rendus (Paris) **160**, 302 (1915).
[23] http://en.wikipedia.org/wiki/Fractal.
[24] T. Vicsek, *Fractal Growth Phenomena* (World Scientific, Singapore, 1992).
[25] P. Meakin, Annu. Rev. Phys. Chem. **39**, 237 (1988).
[26] T. A. Witten, Jr., and L. M. Sander, Phys. Rev. Lett. **47**, 1400 (1981).
[27] See EPAPS Document No. E-PRLTAO-102-055912 for supplemental details. For more information on EPAPS, see http://www.aip.org/pubservs/epaps.html.
[28] T. R. Welberry, *Diffuse X-ray Scattering and Models of Disorder* (Oxford University Press, New York, 2004).
[29] F. Miyamaru and M. Hangyo, Appl. Phys. Lett. **84**, 2742 (2004).
[30] F. Przybilla *et al.*, Opt. Express **16**, 9571 (2008).
[31] T. Matsui *et al.*, Nature (London) **446**, 517 (2007).